NeuroImage 86 (2014) 480–491

Contents lists available at ScienceDirect

NeuroImage

journal homepage: www.elsevier.com/locate/ynimg

Group-level spatial independent component analysis of Fourier envelopes of resting-state MEG data

Pavan Ramkumar [a,*], Lauri Parkkonen [a], Aapo Hyvärinen [b,c]

[a] Brain Research Unit, Low Temperature Laboratory, Aalto University School of Science, PO Box 15100, 00076 Aalto, Finland
[b] Department of Mathematics and Statistics, Department of Computer Science, University of Helsinki, Helsinki, Finland
[c] Helsinki Institute of Information Technology, Helsinki, Finland

ARTICLE INFO

Article history:
Accepted 20 October 2013
Available online 31 October 2013

Keywords:
Magnetoencephalography
Neural oscillations
Fourier energy
Independent component analysis
Minimum norm estimate
Resting state
Natural stimulation
Inter-subject analysis

ABSTRACT

We developed a data-driven method to spatiotemporally and spectrally characterize the dynamics of brain oscillations in resting-state magnetoencephalography (MEG) data. The method, called envelope spatial Fourier independent component analysis (eSFICA), maximizes the spatial and spectral sparseness of Fourier energies of a cortically constrained source current estimate. We compared this method using a simulated data set against 5 other variants of independent component analysis and found that eSFICA performed on par with its temporal variant, eTFICA, and better than other ICA variants, in characterizing dynamics at time scales of the order of minutes.

We then applied eSFICA to real MEG data obtained from 9 subjects during rest. The method identified several networks showing within- and cross-frequency inter-areal functional connectivity profiles which resemble previously reported resting-state networks, such as the bilateral sensorimotor network at ~20 Hz, the lateral and medial parieto-occipital sources at ~10 Hz, a subset of the default-mode network at ~8 and ~15 Hz, and lateralized temporal lobe sources at ~8 Hz.

Finally, we interpreted the estimated networks as spatiospectral filters and applied the filters to obtain the dynamics during a natural stimulus sequence presented to the same 9 subjects. We observed occipital alpha modulation to visual stimuli, bilateral rolandic mu modulation to tactile stimuli and video clips of hands, and the temporal lobe network modulation to speech stimuli, but no modulation of the sources in the default-mode network.

We conclude that (1) the proposed method robustly detects inter-areal cross-frequency networks at long time scales, (2) the functional relevance of the resting-state networks can be probed by applying the obtained spatiospectral filters to data from measurements with controlled external stimulation.

Introduction

During the past decade, the characterization of resting-state brain networks (RSNs) and their dynamics has become an important field of study (Damoiseaux et al., 2006; Fox and Raichle, 2005). A comprehensive meta-analysis of fMRI studies by Smith et al. (2009) suggests that brain networks active during complex stimulation or task performance were very similar to the networks active during rest. Given that the majority of RSN studies have characterized metabolic variations using positron emission tomography (PET) or hemodynamics using functional magnetic resonance imaging (fMRI), it would certainly be beneficial to characterize RSN dynamics using direct non-invasive measures of neural activity such as electro- or magnetoencephalography (EEG/MEG). One characteristic feature of resting-state networks (RSNs) obtained from fMRI data is that they exhibit inter-areal correlations in the blood oxygenation level dependent (BOLD) signal.

Invasive studies have identified robust inter-hemispheric gamma power correlations between the auditory cortices (Nir et al., 2008) suggesting a neural basis for the BOLD bilateral auditory network. Non-invasive electrophysiological equivalents of RSNs using electro- or magnetoencephalography (EEG/MEG), or simultaneous EEG and fMRI have also been sought (Goldman et al., 2002; Laufs et al., 2003; Mantini et al., 2007; Moosmann et al., 2003). These studies typically found power correlations between electrophysiological signals and the BOLD signal in different frequency bands, but the spatial distribution of such correlations was found to be limited focally to a few brain areas. More recently, de Pasquale et al. (2010) reported non-invasive seed-based correlations in the dorsal attention network and the default mode network using MEG. Subsequently, robust MEG RSNs comparable to those reported with fMRI were identified across subjects using temporal independent component analysis (Brookes et al., 2011a, 2011b). Knyazev et al. (2011) showed that the spatial patterns of independent components obtained from EEG alpha oscillations overlapped with the posterior sites of the default-mode network. Analysis of spectral properties of EEG temporal independent components and their power

* Corresponding author. Fax: +358 9 470 22969.
E-mail address: pavan@neuro.hut.fi (P. Ramkumar).

1053-8119/$ – see front matter © 2013 Elsevier Inc. All rights reserved.
http://dx.doi.org/10.1016/j.neuroimage.2013.10.032

correlations using graph theoretic measures has revealed strong anterior–posterior alpha power correlations during the eyes-closed state (Chen et al., 2013).

Independent component analysis (ICA) is a well-established data-driven method for factoring resting-state fMRI data into temporally covarying, spatially independent sources or networks (Beckmann and Smith, 2005; Calhoun et al., 2001). By contrast, in the analysis of EEG/MEG data, ICA has mainly been applied for artifact rejection. However, as we have argued earlier, after suitable transformations of the data (Hyvärinen et al., 2010; Ramkumar et al., 2012), ICA is the prime candidate for data-driven characterization of oscillatory EEG/MEG activity. In earlier work we have shown that the ICA cost function is more selective to the statistical properties of the oscillatory sources after a sparsifying transform of the data. First, we proposed that applying complex-valued ICA to short-time Fourier transforms (STFTs) of MEG signals is likely to reveal physiologically meaningful components (Hyvärinen et al., 2010). We have referred to this method as Fourier-ICA, but for distinction from other methods here we call it temporal Fourier-ICA (TFICA). Subsequently, we extended complex-valued ICA on STFTs from the sensor space to source space and further argued the advantage of imposing spatial and spectral sparseness on the Fourier coefficients to exploit prior knowledge on the nature of cortical oscillations. We have referred to this method as spatial Fourier-ICA (SFICA) (Ramkumar et al., 2012).

Conventional methods in time–frequency analysis (Boonstra et al., 2007; Dalal et al., 2008; Düzel et al., 2003; Hoogenboom et al., 2006; Jensen and Tesche, 2002) typically require pre-specification of a frequency band and/or a time window around an event of interest. Using these methods, it is not obvious how to combine information across frequency bands, especially in multi-channel recordings, or how to analyze spontaneous activity in long recordings. By comparison, the advantage of data-driven methods such as TFICA and SFICA is that they automatically extract narrowband oscillations from broadband data without having to manually specify a frequency band of interest. However, with TFICA/SFICA we have mainly found components expressing activation in a single region as opposed to connectivity across multiple regions. To specifically address this shortcoming of Fourier-based methods, we hypothesized that the resting-state connectivity is manifested in the envelope correlations between oscillatory dynamics across brain regions. One motivation of the envelope-based methods is the recent success of de Pasquale et al. (2010) and Brookes et al. (2011b) in the identification of electrophysiological RSNs from seed-based envelope correlations and ICA of narrowband envelopes, respectively.

The focus of the article is threefold. First, we intend to develop and validate using simulations, a method based on independent component analysis, to estimate electrophysiological resting-state networks in source-space as opposed to individual sources. Second, we intend to apply the method to real MEG data to understand how networks identified during the resting state are modulated during natural stimulation. We propose to apply real-valued TFICA or SFICA on the broadband Fourier spectra (magnitudes of the Fourier coefficients) rather than complex-valued ICA on the complex-valued Fourier coefficients. We call these methods envelope SFICA (eSFICA) or envelope TFICA (eTICA). After benchmarking these envelope methods against the other ICA-based variants using a realistic simulated dataset, we analyze how MEG resting-state oscillatory networks are modulated by stimulation.

Materials and methods

Simulated data

We designed a realistic simulated dataset to test the various ICA-based source separation algorithms using the following methodology. We pre-selected 10 seed regions and placed a current dipole in each of them. The dipoles were oriented normal to the local cortical surface. Source strengths were amplitude-modulated sinusoids at pre-selected carrier frequencies. Fig. 1 gives a list of these sources along with their spatial locations indicated on the inflated brain, the time-courses of their envelopes, their spectra, and their MNI coordinates and carrier frequencies. The amplitude-modulated time courses (duration: 2 min and sampling rate: 150 Hz) were generated as follows.

1) The carrier signal was generated by adding uniformly distributed noise to a pure sinusoid of a specified frequency. The standard deviation of the noise was set to 0.05 times the standard deviation of the sinusoid. Since this relatively low-amplitude noise introduces a phase jitter to the sinusoid, we refer to this noise as phase noise. The small jitter introduced by the phase noise spreads the spectral peak, thus making the signal better mimic a cortical oscillation.
2) The envelope was generated as follows.
   a) A spike train (simulating e.g. a thalamic pacemaker signal) was modeled as a random binary sequence. We used a temporal sparseness parameter of 0.01 which indicates that 1% of the binary sequence was populated by 1's and the rest by 0's. At the same sampling rate of 150 Hz, this leads to a sequence with 0.67 spikes per second.
   b) To mimic the process of temporal summation of the thalamic drives arriving at the cortex, we used a basis set of 6 Gaussian functions with an 8-s temporal support. The 6 standard deviations of the Gaussian basis functions were integral multiples of 0.27 s, ranging up to 1.6 s.
   c) The temporal summation process itself was modeled as a convolution. Specifically, the spike train was then convolved with each Gaussian function in the basis set, and these convolved signals were summed together with random weights (loadings of the basis set) constrained to have a unit sum. Together, the sparseness of the spike train and the standard deviations of the Gaussian basis functions determined the temporal sparseness of the envelope.
3) The carrier signal was multiplied by the envelope to generate the amplitude-modulated signal.
4) Pink noise (1/f noise) was added such that the standard deviation of the noise was 10% of that of the amplitude-modulated signal to mimic brain noise, which is observed, for instance, in local field potentials (Buszaki, 2009).
5) Finally, the noisy amplitude-modulated signal was constrained to have unit variance.

Thus, each oscillatory source was specified by 14 parameters:

1) Location (orientation perpendicular to the local cortical surface)
2) Carrier frequency of the oscillation
3) Phase-noise variance
4) Temporal sparseness of the spike train
5) The Gaussian basis parameters (basis cardinality, temporal support and spread)
6) The Gaussian basis loadings (weights to combine basis-convolved spike train)
7) Pink-noise level.

Parameters other than location, carrier frequency and the 6 basis loadings were identical for all 10 sources. The parameters were selected so that a simulated source signal visually resembled a real MEG signal.

Importantly, not all sources were independently generated. Rather, we simulated two types of interactions between sources:

1. Envelope correlation (identical envelope but independent carrier signal)
2. Envelope anticorrelation (envelope with a Pearson correlation coefficient of −1 to the original envelope, and independent carrier signal).

The interactions between the sources were symmetric; see Table 1.

After the time series of all the sources were generated as described above, a MEG measurement on the 306-channel Vectorview sensor array (Elekta Oy, Helsinki, Finland) was simulated by computing the

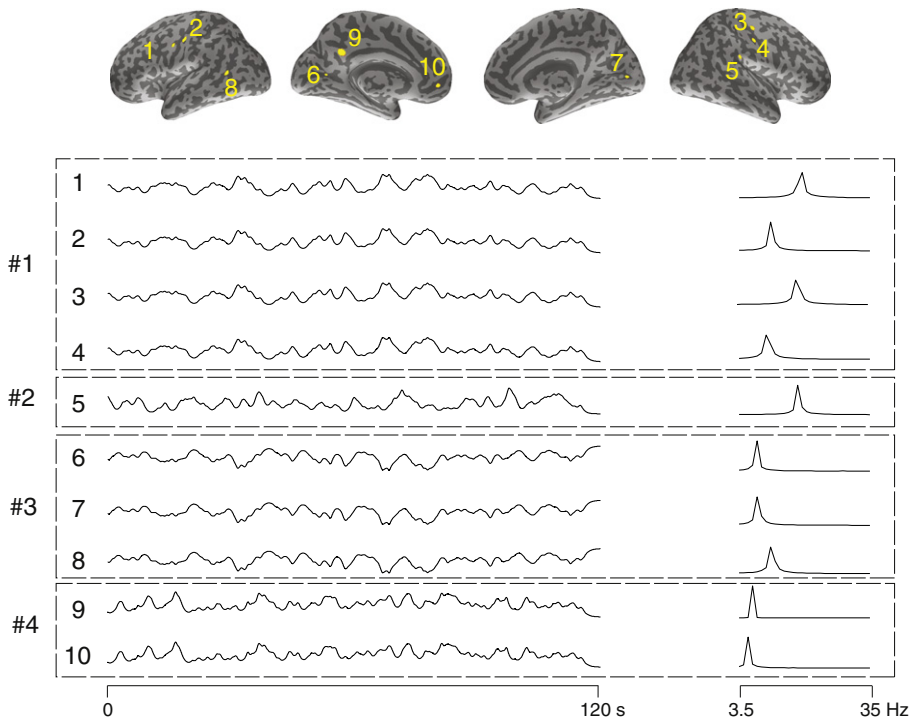

	Region	MNI Coordinates (x y z, mm)	Frequency (Hz)
1	Left central sulcus (MI)	−53.2 3.4 35.2	19.5
2	Left central sulcus (SI)	−46.5 13.3 41.9	12.0
3	Right central sulcus (MI)	40.7 −16.9 55.5	19.2
4	Right central sulcus (SI)	49.3 −17.2 37.0	11.0
5	Right posterior parietal operculum (SII)	58.0 −35.4 28.4	19.0
6	Left calcarine sulcus (V1)	−25.9 −71.8 7.4	8.0
7	Right central sulcus (V1)	12.4 −89.7 4.0	8.5
8	Left lateral middle temporal area (MT)	−42.9 −52.7 5.4	12.1
9	Left posterior cingulate cortex (PCC)	−5.5 −48.1 30.1	7.0
10	Left medial prefrontal cortex (MPFC)	−41.5 69.0 64.6	6.0

Fig. 1. Top: Locations of the simulated oscillatory current sources on an inflated and flattened brain surface. Center: Envelopes and power spectra of each source. Sources 1–4 constitute network #1, source 5 network #2, sources 6–8 network #3, and sources 9–10 network #4. Bottom: Brain regions, Montreal Neurological Institute (MNI) co-ordinates and carrier frequencies.

corresponding dipolar fields using a single-compartment BEM conductor model with 20,480 triangles. Finally, noise was added from a real measurement with a similar sensor array in the absence of a subject at a level of −10 dB with respect to the simulated MEG data.

Real MEG data

We used the data set presented in our earlier study (Ramkumar et al., 2012). Briefly, we used MEG data obtained with the 306-channel Vectorview system from 9 healthy subjects (5 females, 4 males, age range 23–41 years) during 10 min of alert resting (eyes open, fixating on a crosshair) and 12 min of natural stimulation. The stimuli comprised 6–33 s video clips of faces (4 blocks), hands (2 blocks), and outdoor scenes (3 blocks); recordings of a male voice narrating the history of the local university (3 blocks) and guitar-playing instructions (3 blocks); short pure tones (3 blocks), and bilateral tactile stimulation to the fingertips (7 blocks). Pure tones were delivered in 0.1-s beeps at 250, 500, 1000, 2000 or 4000 Hz (Malinen et al., 2007). Tactile stimuli were delivered using pneumatic diaphragms at 4 Hz to the four fingers excluding the thumb, in a randomized order, such that homologous fingers were stimulated simultaneously (Ramkumar et al., 2012). Each stimulus block alternated with a 15-s rest block. The sequence in which blocks were presented was pre-randomized but identical across sessions and subjects. Along with MEG, a diagonal electrooculogram (EOG) was also

Table 1
Interaction between source envelopes. Envelopes are either correlated (+) or anti-correlated (−). While the envelopes are strongly correlated, the amplitude-modulated timecourses are completely uncorrelated. Sources 1–4 constitute network #1, source 5 constitutes network #2, sources 6–8 constitute network #3, and sources 9–10 constitute network #4.

	1	2	3	4	5	6	7	8	9	10
1		+	+	+		−	−	−		
2	+		+	+		−	−	−		
3	+	+		+		−	−	−		
4	+	+	+			−	−	−		
5										
6	−	−	−	−			+	+		
7	−	−	−	−		+		+		
8	−	−	−	−		+	+			
9										+
10									+	

measured, with one electrode above the left eye and another electrode below the right eye.

Pre-processing

We pre-processed the data identically as in our earlier work (Ramkumar et al., 2012) with signal space separation (SSS) (Taulu and Kajola, 2005) followed by a custom routine for removing occasional discontinuities (DC jumps) in the data.

Source localization of short-time Fourier transforms

First, we computed 1-s non-overlapping Hamming-windowed short-time Fourier transforms at the sensor level.

For each subject, the brain's cortical surface was reconstructed from an anatomical MRI using Freesurfer (http://surfer.nmr.mgh.harvard.edu, Martinos Center for Biomedical Imaging, Massachusetts General Hospital). We then projected the complex-valued short-time Fourier transformed data to the cortical surface by left-multiplying a linear inverse operator (an average of 5 mm separation between source points for simulated data, and 15 mm for real MEG data). The linear inverse operator was computed using minimum norm estimation (MNE) with depth weighting and noise normalization (often referred to as dynamic statistical parametric mapping or dSPM; see Dale et al., 2000). We used the implementation in the free MNE package available at: http://www.nmr.mgh.harvard.edu/martinos/userInfo/data/sofMNE.php. We retained only the current estimate in the direction normal to the cortical surface. Although low frequencies (<4 Hz) have been implicated in various physiological and cognitive functions, certain methodological issues need to be addressed to take them into account in our method. For example, given the power-law distribution of the noise spectrum of MEG, the noise covariance required in inverse modeling would have to be estimated separately for higher and lower frequencies. Thus, to avoid the disproportionate emphasis on near-DC fluctuations, we discarded the first 3 Fourier bins corresponding to 0–3.5 Hz before further analysis. In addition to cortical-level STFTs, we also projected the raw sensor-level time series (without computing STFTs) to obtain cortical-level time series.

To test the robustness of our method to assumptions about the forward model, we used a coarser BEM model (5120 triangles) and a different source point set that excluded exact matches to the simulated source locations to analyze the simulated dataset. This allowed us to test our method under conditions when the forward model is not well chosen. Further, for the simulated data, the source localization was performed directly on the canonical Montreal Neurological Institute (MNI) brain. For real MEG data, we first performed the source localization on individual subjects' brains and then projected the cortical-level single-subject data to the MNI brain using a surface-based morphing algorithm (Fischl et al., 1999).

Blind source separation

Having estimated the space–time–frequency tensor of oscillatory currents at the cortical level, we applied six blind source separation methods to identify functionally distinct networks. After evaluating the results of these methods on the simulated data, we selected the most interesting method to apply on real MEG data.

Fourier ICA

Fourier-ICA, as well as the other methods below, was applied in temporal and spatial form. For TFICA and SFICA, we employed the classical noiseless linear mixture model for independent component analysis given by $\mathbf{X} = \mathbf{AS}$, where $\mathbf{X}$ is the complex-valued STFT tensor (time × source points × frequency bins) arranged as a matrix. $\mathbf{A}$ and $\mathbf{S}$ were estimated using the complex-valued FastICA algorithm (Bingham and Hyvärinen, 2000). For TFICA, the tensor was arranged as a matrix of source points × short-time Fourier transforms. ICA on this matrix maximizes independence in the time–frequency domain. The rows of the estimated components $\mathbf{S}$ give independent time–frequency atoms, which are then converted into time courses and power spectra by taking the absolute values and averaging over frequency bins and time windows, respectively. The absolute values of the columns of the estimated mixing matrix $\mathbf{A}$ give the spatial maps corresponding to the independent time–frequency atoms. The estimation and interpretation was identical to those in our previous work (Hyvärinen et al., 2010) except that we operated here at the cortical source rather than at the sensor level. We chose to apply TFICA at the cortical level to facilitate a more direct comparison with other methods. For SFICA, the tensor was rearranged by concatenating the Fourier coefficients for each source point into a row vector for each time window. ICA on this matrix maximizes independence in spatiospectral domain simultaneously. The estimation and interpretation was exactly as in our previous work (Ramkumar et al., 2012). Fig. 2 illustrates the data matrix representation prior to TFICA (left) and SFICA (right).

Envelope Fourier-ICA

For the envelope-based methods, we applied the same linear mixture model after taking the absolute value of the Fourier coefficients, resulting in $|\mathbf{X}| = \mathbf{AS}$. The arrangements of the tensor $\mathbf{X}$ for envelope TFICA and envelope SFICA were identical to TFICA and SFICA, respectively.

Ordinary ICA

For comparison, we also applied ordinary ICA, i.e. instead of decomposing the original tensor, we applied temporal and spatial independent component analysis (TICA and SICA) to the spatiotemporal data without going to a Fourier representation. Fig. 3 illustrates the manner in which the data matrix is represented prior to TICA (left) and SICA (right).

Once the independent components were estimated, we ranked them by the variance of the columns of the mixing matrix $\mathbf{A}$.

To reiterate, all the evaluated algorithms comprised two steps: Step 1, a distributed source localization method to obtain cortically-constrained current estimates; Step 2, a variant of independent component analysis (ICA) to separate the sources into oscillatory networks. We investigated the relative merits of 6 variants of ICA: spatial and temporal envelope Fourier ICA, spatial (Ramkumar et al., 2012) and temporal (Hyvärinen et al., 2010) complex-valued Fourier-ICA, and 2 non-Fourier-ICA methods: ordinary spatial and temporal ICA. We compared the performance using 5 different metrics (see Section Evaluation of algorithms on simulated data). We then repeated this comparison 10 times by simulating the dataset with different phase noise and additive pink noise for each source, as well as a different empty-room measurement added as sensor noise for each repeat.

In each case, before applying ICA, we reduced the data to K dimensions ($K = 25$ for the simulated data; $K = 40$ for the real MEG data)

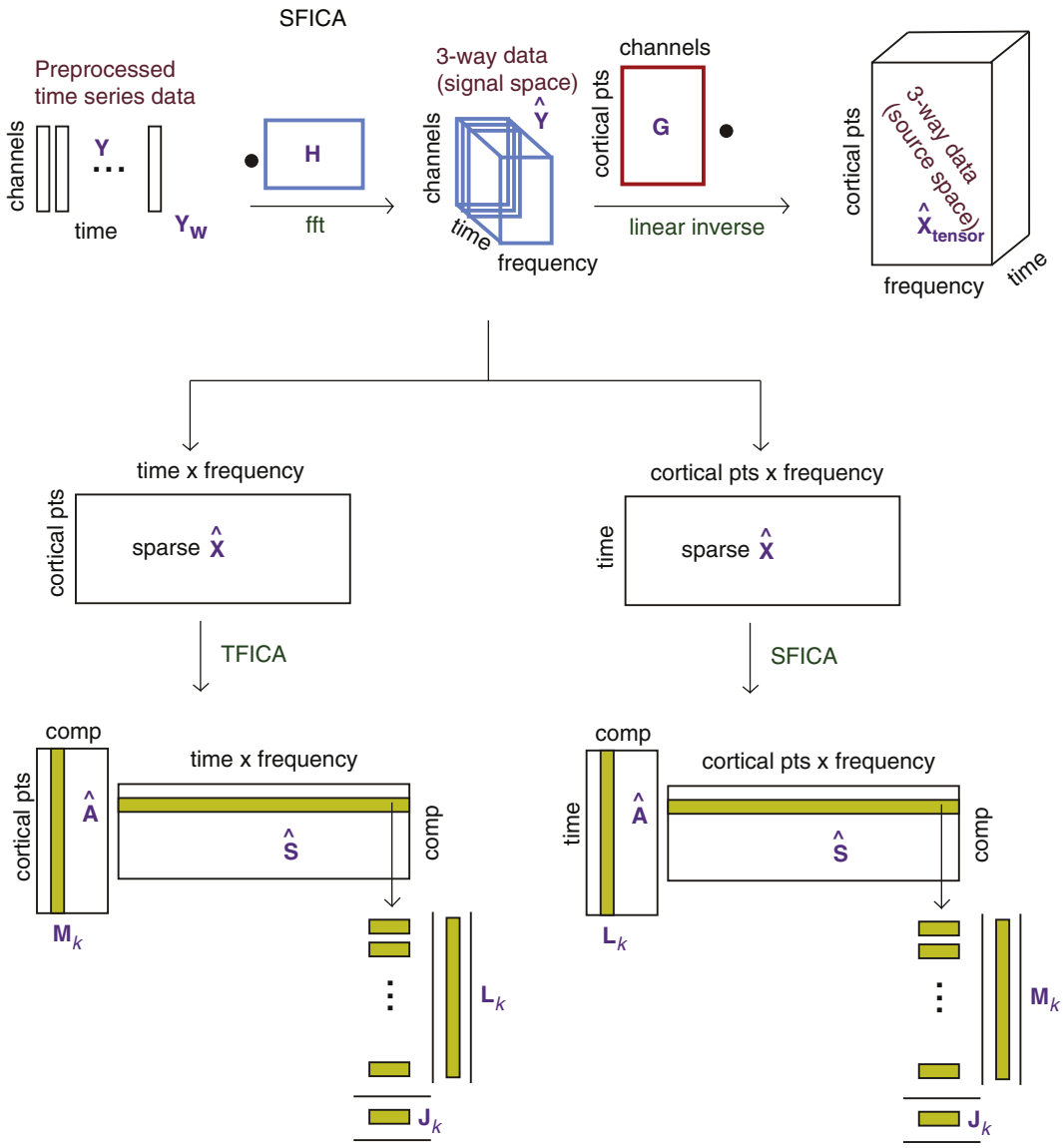

Fig. 2. Illustration of the data matrix representation in temporal Fourier-ICA (TFICA) and spatial Fourier-ICA (SFICA) (right). The preprocessed time-series data (**Y**) was windowed (**Yw**) and right-multiplied by the FFT matrix to obtain channel-wise short-time Fourier transforms ($\hat{\mathbf{Y}}$). The STFTs were left-multiplied by the precomputed linear inverse operator (**G**) to obtain 3-way data in cortical space ($\hat{\mathbf{X}}$). Left: The complex valued $\hat{\mathbf{X}}$ was rearranged as cortical points vs. time × frequency (TFICA), and complex-valued ICA was applied. The absolute values of the columns of **A** provide the spatial power maps ($\mathbf{M}_k$) and the rows of $\hat{\mathbf{S}}$ can be decomposed into the envelopes of Fourier power ($\mathbf{L}_k$) and power spectra ($\mathbf{J}_k$) respectively. Right: The complex-valued $\hat{\mathbf{X}}$ was rearranged as time vs. cortical points × frequency (SFICA) and complex-valued ICA was done on this matrix. The squared absolute values of the rows of **^S** provide the envelopes of Fourier-power and the rows of **A** can be decomposed into the spatial power map and power spectra.

using principal component analysis (PCA) followed by whitening in the following step. The choice of PCA dimension was based on fMRI studies (Abou-Elseoud et al., 2010; Smith et al., 2009) which suggest the choice of a dimension slightly larger than the expected number of underlying sources. Although information theoretic methods such as Akaike information criterion or Bayesian information criterion exist, such rules of thumb seem to be more commonly adopted during dimensionality reduction of neuroimaging data. In the case of simulated data, we knew the number of underlying sources to be 10 and therefore chose 25. In the case of real MEG data, we assumed the underlying number of sources to be 30 and therefore chose 40.

Evaluation of algorithms on simulated data

An ideal method would correctly identify the locations of the sources, their power spectra, and their temporal envelopes. It should also capture the interactions between those sources by grouping sources belonging to one network into the same component. With these general objectives in mind, we focused on temporal and spectral reconstruction, and the effectiveness of network detection. We did not emphasize the accuracy of source localization as much as the effectiveness of network detection because the accuracy of localization is largely dependent on the applied distributed source localization method.

Temporal similarity

For each component, we computed the temporal correlation coefficients between its estimated envelope time course and all true envelopes of the 10 simulated sources. The maximum absolute correlation coefficient was considered to indicate the best matching simulated source. To obtain a concise summary over components, we then took the mean of this maximum absolute correlation to quantify temporal similarity.

Spectral similarity

We computed the power spectrum of all simulated sources (computed as the mean of the non-overlapping 1-s Hamming windowed

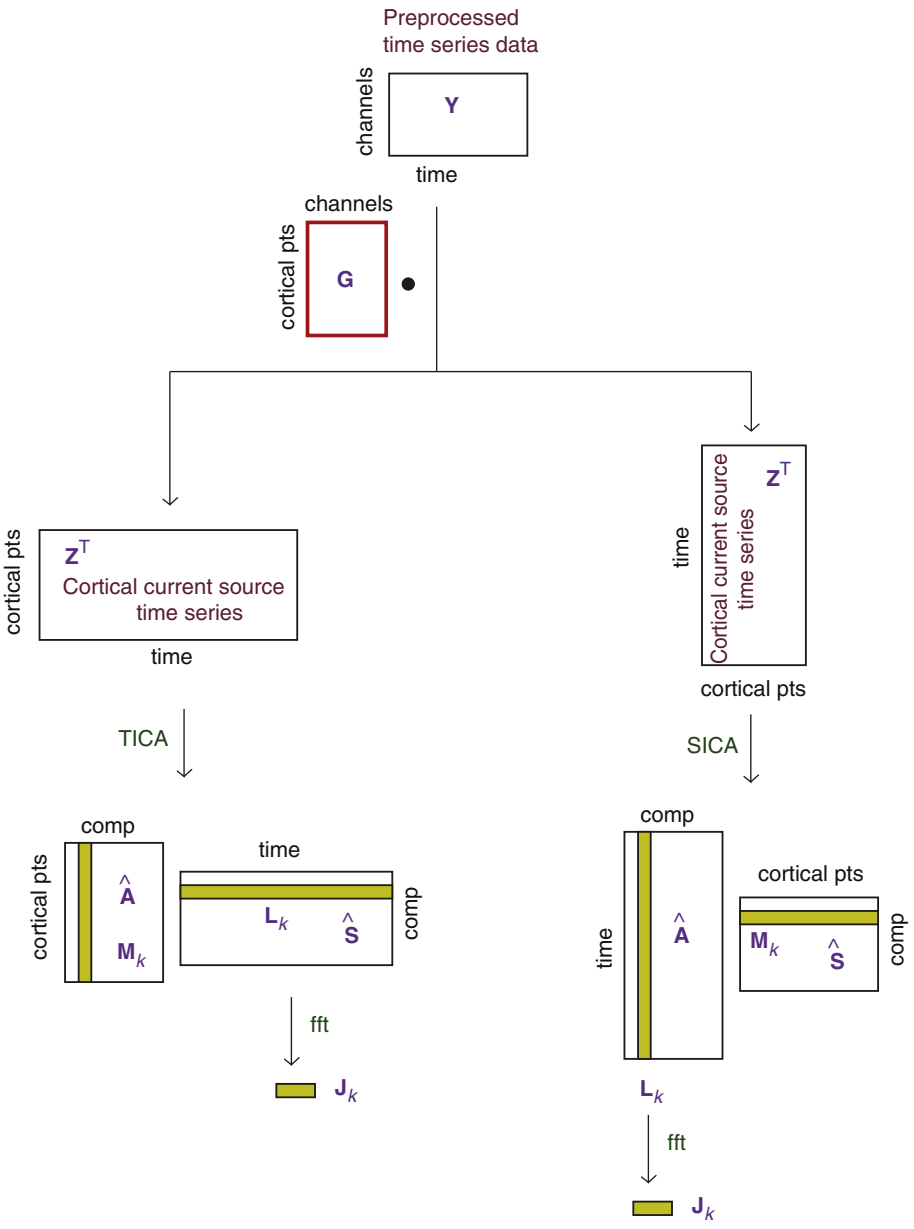

Fig. 3. Illustration of the data matrix representation in ordinary TICA (left) and SICA (right). The preprocessed time-series data matrix (**Y**) was left-multiplied by the precomputed linear inverse operator (**G**) to obtain the cortical current time-series (**Z**). Real-valued ICA was applied to the appropriately oriented matrix in each case. Left: The columns of **A** provide the spatial maps ($\mathbf{M}_k$) and the rows of $\hat{\mathbf{S}}$ provide the time courses ($\mathbf{L}_k$) and their FFT amplitudes are then taken to represent the power spectra ($\mathbf{J}_k$). Right: The rows of $\hat{\mathbf{S}}$ provide the spatial maps ($\mathbf{M}_k$) and the columns of **A** provide the time courses ($\mathbf{L}_k$). As before the FFT of $\mathbf{L}_k$ represents the power spectra ($\mathbf{J}_k$).

short-time Fourier transforms). Just as for the temporal similarity metric, for each component, we computed the correlation coefficients between its estimated power spectrum and the true spectra of all 10 simulated sources. The maximum absolute value among these 10 correlation coefficients was considered to indicate the best matching simulated source. As before, we took the mean of this maximum absolute correlation across components to measure the spectral similarity.

Effectiveness of network detection

To compare the ability to identify networks, we first computed a template for each network as follows. We simulated the MEG field produced by each dipolar point source belonging to the network, projected the field back to the cortical surface using a dSPM inverse operator (see Section Source localization of short-time Fourier transforms), and then summed up all inverse projections of the sources belonging to the given network. Such a template can be treated as a point-spread function of the source, and it factors out the localization errors produced by the distributed inverse modeling method. Thus, any deviation from this template could be attributed to the effects of the empty room measurement noise and the source separation algorithm. We then computed for each of the 4 networks, the spatial correlation between the template map and the spatial map of all estimated independent components. The component with the largest correlation was considered to best represent the network. This correlation coefficient was treated as a metric of network detection and subsequently compared across the various ICA methods. A larger score indicates a method that better identifies networks.

Analysis of real MEG data

Based on the results from the simulations (see Section Results on simulated data), we selected eSFICA to be applied on resting-state

MEG data and studied the dynamics of the estimated components during natural stimulation. First, we performed the source-localization of the raw time-series data as well as the STFTs using minimum-norm estimation in the same way as in the simulation; see Section Source localization of short-time Fourier transforms.

Group ICA by two-stage reduction

We applied ICA to a group-level representation of the resting-state MEG data from 9 subjects, obtained by a two-stage reduction (Calhoun et al., 2001). In the first stage, we reduced the data from each subject to 40 dimensions using PCA and whitened them. In the second stage, we temporally concatenated the reduced data from all subjects, and reduced the dimensionality again to 40 using PCA. We then estimated as many components as the dimensionality (i.e. 40) using FastICA.

Selecting consistent components from replicates

We applied ICA as above to resting-state data acquired in a second session from the same 9 subjects. Independent components found to be sufficiently similar in both sessions were retained for further analysis. To set an appropriate threshold for the correlation, we measured this correspondence by a statistical test derived from a specific null hypothesis (Hyvärinen, 2011). Under this null hypothesis, we assume that the ICA demixing matrix is a random orthogonal matrix; the goal of the statistical test is then to estimate how likely two components correspond across sessions by chance. We set a Bonferroni-corrected false positive rate of $\alpha = 0.05$. Only those components that rejected the null hypothesis were retained for further analysis. For each such component, we computed the correspondence score across sessions as the correlation coefficient between the independent component vectors.

Reconstruction of dynamics during natural stimulation from resting-state spatiospectral filters

Each independent component estimated from resting-state data can be considered as a linear "spatiospectral" filter, which describes an oscillatory network with a certain spatial pattern of activity. We applied these filters (one for each component) to the short-time Fourier transform of the natural-stimulation data of each subject.

Modulation of amplitude envelope by external stimuli

How do external stimuli modulate networks identified during rest? We addressed this question for each stimulus type, time course (component) and subject, separately as follows. For the 6 different types of stimuli, viz. (1) auditory pure tones, (2) natural speech (with university history and guitar instruction blocks lumped together), (3) videos of faces, (4) of hand actions, (5) of natural scenes, and (6) periodic tactile stimuli, we computed the *modulation depth* for each temporal profile (estimated envelope time course or instantaneous amplitude) as the percentage difference of the mean signal in the stimulus block and the mean signal from a 15-s baseline epoch preceding the stimulus block. For a given stimulus type, modulation depths were computed block-by-block and then averaged across all blocks of that type over the entire time course. We then tested whether this quantity was normally distributed across subjects. A Kolmogorov–Smirnov test to compare the mean-removed, variance-normalized modulation depth against a standard normal distribution could not reject the null hypothesis. We then performed the following second-level analyses on the modulation depths. First, for each component, we performed univariate two-tailed *t*-tests for each stimulus type to determine the modalities for which a component was modulated significantly differently ($p < 0.01$) from zero. Second, to study the specificity of the network to a certain subset of the stimuli, we performed a repeated measures analysis of variance (ANOVA) to assess whether there was a difference in modulation depths across stimulus types. Components that showed a significant difference of modulation depth ($p < 0.05$) between stimulus types were labeled "Specific".

Testing for eye-movement artifacts

To test the possibility that some components were related to eye-movement artifacts, we computed correlations between the absolute value of the electrooculogram (EOG) with the time course of each component obtained by applying the spatiospectral filter to the natural stimulation data (after downsampling to 1 Hz), separately for each subject. For each component, we performed a univariate two-tailed *t*-test to examine whether its time course was statistically significantly ($p < 0.05$) correlated with the EOG envelope (absolute value of the time course).

Visualization

Each independent component represents a spatiospectral filter, i.e. the set of Fourier powers concatenated across source points. We computed the spatial profile (map) by averaging the independent component across the Fourier bins for each source point. The spatial maps were thresholded at the 95th percentile. We computed the positive and negative spectral profiles by averaging the independent component across source points exceeding the 95th percentile threshold in positive and negative directions respectively. Although the independent components were calculated from 3.5 to 75 Hz, the power spectra were only visualized from 3.5 to 40 Hz because the spectra had extremely small values in the range 40–75 Hz. Finally, we plotted the modulation depths for each stimulus modality as bars, along with error bars representing the standard errors of mean (SEM) across the 9 subjects.

Results

Results on simulated data

Table 2 shows the metrics for temporal and spectral similarity and the 4 network detection metrics for the 6 different ICA algorithms.

Table 2
Comparison of the six source separation algorithms. Each column represents one method. The rows represent the metric describing the overall temporal similarity, overall spectral similarity, and the detectability of an individual network (mean ± SD across 10 simulation repeats; see Section Evaluation of algorithms on simulated data in the text for details). The last two rows give the mean of network detectability and the grand mean score across all metrics.

	Spatial			Temporal		
Metric	eSFICA	SFICA	SICA	eTFICA	TFICA	TICA
Temporal similarity	0.17 ± 0.04	0.17 ± 0.05	0.18 ± 0.03	0.14 ± 0.01	0.15 ± 0.06	0.18 ± 0.03
Spectral similarity	0.48 ± 0.02	0.75 ± 0.01	0.79 ± 0.01	0.27 ± 0.07	0.66 ± 0.01	0.54 ± 0.01
Detection of network 1	0.71 ± 0.05	0.62 ± 0.03	0.02 ± 0.00	0.73 ± 0.01	0.69 ± 0.04	0.02 ± 0.00
Detection of network 2	0.69 ± 0.03	0.57 ± 0.02	0.02 ± 0.00	0.82 ± 0.00	0.67 ± 0.04	0.02 ± 0.00
Detection of network 3	0.69 ± 0.01	0.38 ± 0.06	0.05 ± 0.01	0.80 ± 0.00	0.33 ± 0.05	0.04 ± 0.00
Detection of network 4	0.71 ± 0.02	0.48 ± 0.05	0.02 ± 0.00	0.70 ± 0.00	0.63 ± 0.03	0.02 ± 0.00
Detection of networks (mean)	0.70 ± 0.03	0.51 ± 0.04	0.03 ± 0.00	0.76 ± 0.00	0.58 ± 0.04	0.03 ± 0.00
Grand mean score	0.57 ± 0.03	0.49 ± 0.04	0.18 ± 0.01	0.58 ± 0.02	0.52 ± 0.04	0.14 ± 0.01

Mean and standard deviation are reported across the 10 repeats. The two envelope methods performed better than the other methods, especially in network detection. However, among the envelope methods, eSFICA and eTFICA were statistically indistinguishable. We then decided to focus on eSFICA simply because it has not been reported in the literature previously.

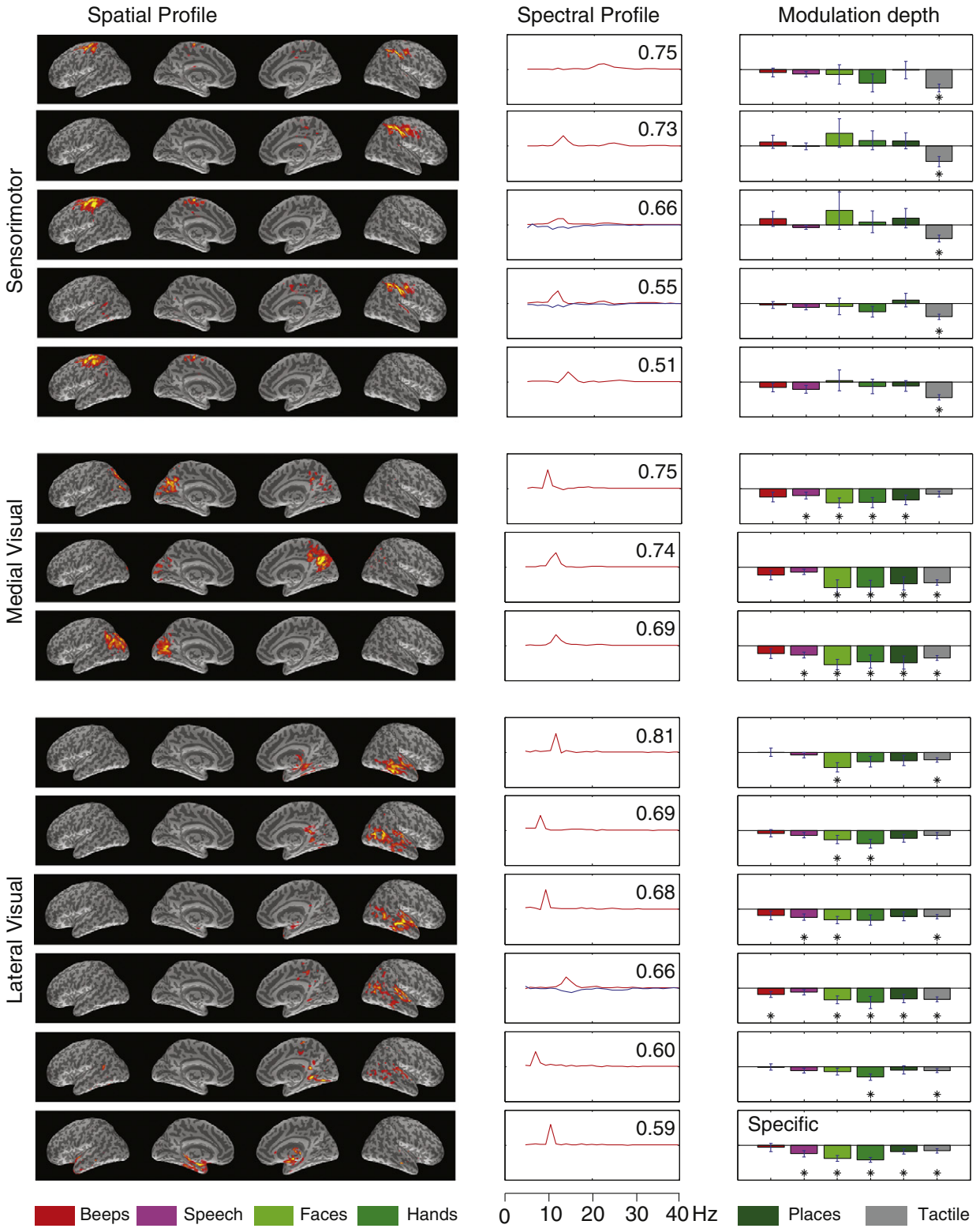

Fig. 4. First 3 component groups: eSFICA spatiospectral filters obtained from resting-state data (left and middle panels) used to interrogate brain dynamics during natural stimulation (right panel). Left: The spatial profiles obtained by averaging the independent component across the Fourier bins. The maps are thresholded at the 95th percentile. Middle: The (positive and negative) spectral profiles are obtained by averaging the independent component across source points exceeding the 95th percentile threshold in positive and negative directions, respectively. The inset shows consistency of the spatiospectral filter across two resting-state sessions as measured by Pearson's correlation coefficient. Right: The modulation depths for each stimulus category are estimated from the temporal profile and averaged across subjects. Error bars show standard errors of mean. A star indicates that the component is modulated significantly differently ($p < 0.05$; uncorrected) from zero. The label "Specific" suggests that there are statistically significant differences ($p < 0.05$) between effect sizes of different stimulus categories. We manually ordered the components according to the dominant modality as sensorimotor, medial visual and lateral visual components.

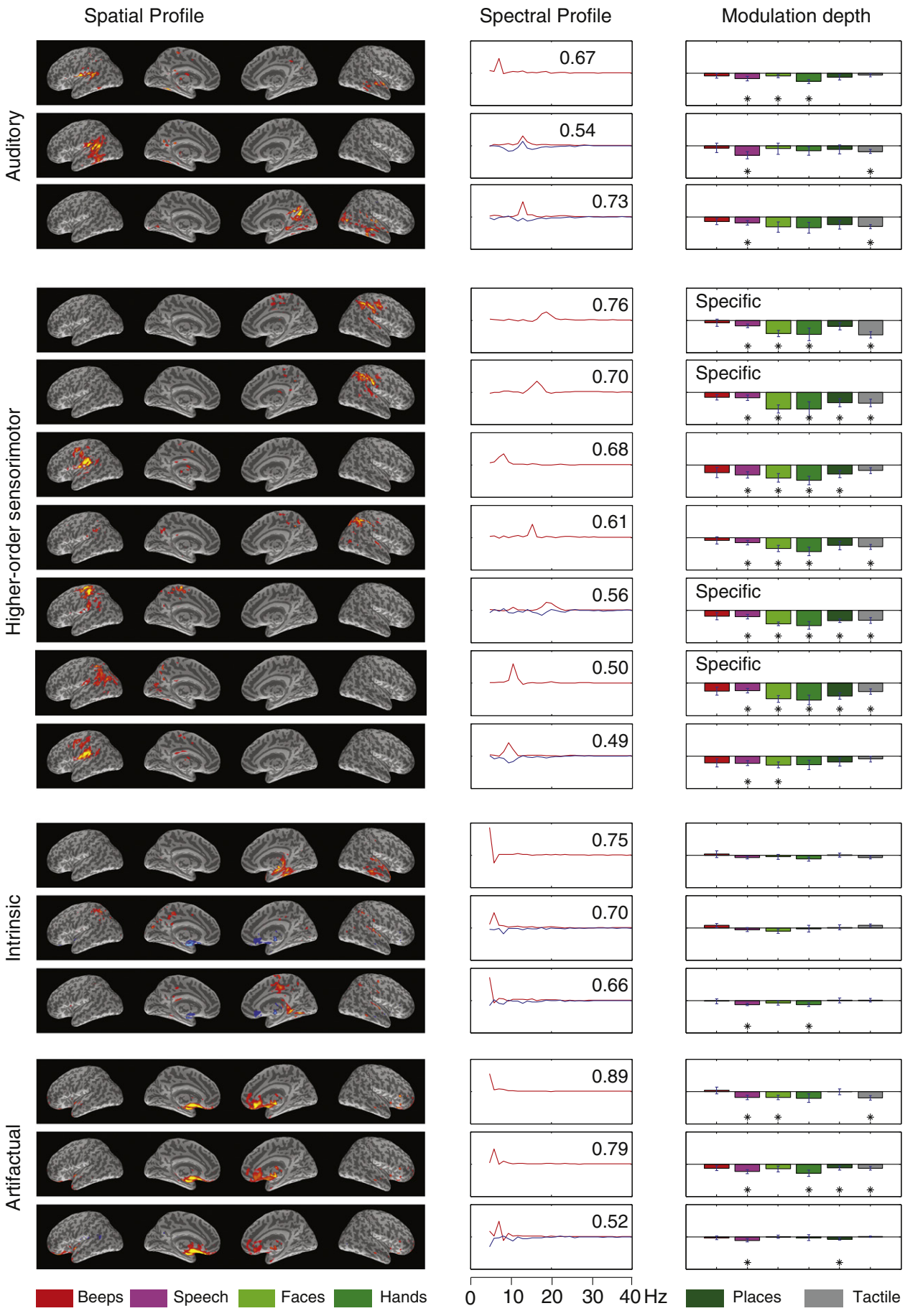
Spatial Profile
Spectral Profile
Modulation depth
Auditory
Higher-order sensorimotor
Intrinsic
Artifactual
0.67
0.54
0.73
0.76
0.70
0.68
0.61
0.56
0.50
0.49
0.75
0.70
0.66
0.89
0.79
0.52
Specific
Specific
Specific
Specific
Beeps
Speech
Faces
Hands
0
10
20
30
40 Hz
Places
Tactile

Results on real MEG data

Figs. 4 and 5 show the estimated resting-state components: their spatial and spectral profiles, as well as their modulation by natural stimuli. Based on the modulation depths and the spatial profiles, we manually rearranged the components into sensorimotor, medial visual, lateral visual, auditory, higher-order sensorimotor, intrinsic, and orbitofrontal (artifactual) components. The grouping is only approximative, and could be contested for several components. However, instead of creating a 'miscellaneous' category for such components, we prefer to assign each component to the closest cluster. In the following, we make some remarks about the components.

Sensorimotor components

We found two unilateral ~10-Hz, two unilateral ~15-Hz, and one bilateral ~20-Hz sensorimotor components (Fig. 4, top panel) spanning the primary somatosensory and motor cortices, as well as the supplementary motor areas (SMA): these were statistically significantly modulated by tactile stimuli alone.

Medial visual components

We observed one bilateral and two lateralized medial parieto-occipital components at ~10 Hz (see Fig. 4, middle panel). These were modulated non-specifically by speech, faces, hands, scenes, and tactile stimuli. The bilateral component peaked slightly below 10 Hz, whereas the lateralized components peaked slightly above 10 Hz.

Lateral visual components

We also observed several components at ~8–15 Hz with spatial maxima over the ventral temporo-occipital pathways (Fig. 4, bottom panel). Most of these components were individually modulated by at least one visual stimulus category. Hence we classified them as higher-order visual components.

Auditory components

We found one ~8-Hz component with bilateral maxima in the auditory cortices, but this component was modulated by speech, faces and hands. In addition, we found two ~15-Hz components with spatial maxima in the left and right auditory cortex and superior temporal cortex, which were modulated by speech and tactile stimuli (see Fig. 5, top panel). The left hemisphere component was also significantly correlated ($p < 0.05$; $r = 0.14$; mean across subjects) with the EOG envelope.

Higher-order sensorimotor components

We found several ~12–20-Hz components with local maxima in the primary and secondary sensorimotor areas, and posterior parietal cortices (Fig. 5, second panel). However, unlike the sensorimotor components that were modulated only by tactile stimuli, these components were modulated non-specifically by speech, faces, hands, places, and tactile stimuli.

Intrinsic components

We found two lower-frequency (<5 Hz) components with spatial maxima in the posterior cingulate, mid-cingulate and parts of the orbitofrontal cortex (Fig. 5, third panel). We found another low-frequency component in the right anterior inferior temporal cortex that was not significantly modulated by any stimulus category. We classified all these components as intrinsic because they exhibit either weak or no modulation to external stimuli. However, the first and the third intrinsic components were weakly but significantly ($p < 0.05$) correlated with the EOG envelopes ($r = 0.08$ and 0.06 respectively; mean across subjects).

Orbitofrontal components

We found three components with large spatial maxima in the orbitofrontal cortices alone (Fig. 5, bottom panel). Two of these three components showed the largest envelope correlation ($r = 0.17$ and 0.15, respectively; mean across subjects) with the EOG envelopes, and the correlations were statistically significantly ($p < 0.05$) different from zero.

Discussion

In this paper, we compared several variants of ordinary temporal and spatial ICA for the analysis of time–frequency fluctuations of current sources inferred from MEG recordings over the whole brain. We found that both temporal and spatial ICA on the Fourier envelope outperform Fourier-ICA and ordinary ICA when it comes to the identification of correlated networks.

The meaning of independence in the spatial Fourier methods is different from the meaning of independence in standard spatial ICA as applied in fMRI. In spatial ICA, independence can be characterized as lack of systematic spatial overlap. Likewise, in our variant of ICA, the components should have no systematic overlap in the spatio-spectral domain. In other words, two components are allowed to be strongly (systematically) overlapping spatially, if they have very different, e.g. completely non-overlapping spectral profiles; conversely, they can have similar spectral profiles if they are spatially non-overlapping. For example, we could have two components (networks) such that component #1 has 10-Hz oscillations in area A and 20-Hz oscillations in area B, and component #2 has 20 Hz oscillations in area A and 10 Hz oscillations in area B. In the spatio-spectral domain, such components are non-overlapping and thus would be separated by ICA.

Comparison of the algorithms

We did not find a clear difference between the performance of spatial and temporal Fourier methods in estimating the temporal profiles (estimated time courses of the signal envelope or instantaneous amplitudes) of the sources. However, the temporal Fourier methods excel at identifying the corresponding networks. This observation might indicate that the mixing matrices are more accurately estimated than the independent components, suggesting the added value of applying both spatial and temporal source separation methods. It is possible that a hybrid spatiotemporal method, e.g. the one proposed by Stone et al. (2002) for fMRI data, would be able to combine the advantages of both types of methods. The non-Fourier-based methods (SICA and TICA) are poor at estimating networks. This observation could be explained by the fact that these methods impose either temporal or spatial sparseness, whereas most networks seem to exhibit narrowband oscillations and would thus benefit from an imposition of spectral sparseness.

In terms of spectral similarity, the envelope methods appear to perform poorly compared with the non-envelope methods: 0.48 ± 0.02 (eSFICA) compared with 0.75 ± 0.01 (SFICA) and 0.79 ± 0.01 (SICA) and 0.27 ± 0.07 (eTFICA) compared with 0.66 ± 0.01 (TFICA) and 0.54 ± 0.01 (TICA). Thus, it is unclear at present whether a particular variant of ICA excels in all metrics. Further research into the methods and the similarity metrics is required.

Fig. 5. Subsequent 4 component groups: eSFICA spatiospectral filters obtained from resting-state data (left and middle panels) used to interrogate brain dynamics during natural stimulation (right panel). Left: The spatial profiles obtained by averaging the independent component across the Fourier bins. The maps are thresholded at the 95th percentile. Middle: The (positive and negative) spectral profiles are obtained by averaging the independent component across source points exceeding the 95th percentile threshold in positive and negative directions, respectively. The inset shows consistency of the spatiospectral filter across two resting-state sessions as measured by Pearson's correlation coefficient. Right: The modulation depths for each stimulus category are estimated from the temporal profile and averaged across subjects. Error bars show standard errors of mean. A star indicates that the component is modulated significantly differently ($p < 0.05$; uncorrected) from zero. The label "Specific" suggests that there are statistically significant differences ($p < 0.05$) between the effect sizes of different stimulus categories. We manually ordered the components as auditory, higher-order sensorimotor, intrinsic components and artifacts.

Two obvious variants that we did not implement here were envelope versions of TICA and SICA (eTICA/eSICA). The IC time courses obtained by these methods would correspond to envelope time courses, and it would be impossible to estimate the spectral profile of such a component. Of course, one alternative would be to separately implement eTICA and eSICA to narrowband signals at various center frequencies. However, this would essentially leave open the problem of combining results across frequency bands, and as such, would sacrifice the elegance of TICA/SICA and the Fourier-based methods, which automatically detect the interesting frequencies in the data. Further, since we set out to characterize the data in a spatiotemporal and spectral manner, we concluded that these methods could not be fairly evaluated against alternatives. Therefore we decided to leave out eTICA and eSICA from this comparison.

Identified resting-state networks

Our results demonstrated the ~10- and ~20-Hz components of the rolandic sensorimotor mu rhythm (Hari and Salmelin, 1997). Robust inter-hemispheric correlations in the sensorimotor network have been observed in fMRI (Biswal et al., 1995) and in intracranial recordings (Nir et al., 2008). It is interesting to note that the ~20-Hz component, but not the ~10-Hz components, showed a bilateral spatial profile. Early MEG studies indicate that the ~20-Hz oscillation is generated precentrally and appears more related to motor than somatosensory processing whereas the ~10-Hz oscillation is postcentral and associated with processing of tactile information, although both rhythms are modulated by movement and tactile stimulation (for a review see Hari and Salmelin, 1997). Thus, understanding the inter-hemispheric coupling of these two spontaneous rhythms would be useful in further elucidating their role in sensorimotor processing.

The bilateral medial parieto-occipital component was modulated by speech and visual stimuli but not by tactile stimuli, whereas the unilateral component was modulated by tactile stimuli as well. The spatial maxima correspond to previously reported generators of the classical ~10-Hz parieto-occipital alpha rhythm. Most of the identified higher-order visual components in the 8–15-Hz range had the sources in the right lateral temporal lobe.

The bilateral auditory component showed a peak at ~8 Hz which corresponds to the tau rhythm reported in an early MEG study (Tiihonen et al., 1991). In addition to speech, this component was modulated by videos of faces and hands as well. The left and right lateralized temporal lobe components were modulated by speech and tactile stimuli at ~12 Hz. Spontaneous rhythms in the auditory cortex and speech production areas have been linked to speech production and perception networks along with frequency-specific lateralization (Giraud et al., 2007). However, we did not observe any differences in the power spectra between the left and right hemisphere components.

The higher-order sensorimotor components showed peaks at ~10 and ~20 Hz, and were modulated not only by tactile stimuli, but also by visual and speech stimuli. Given that the video clips contained pictures of faces and hand actions, and some speech segments described instructions for guitar fingering, the sensorimotor suppression to these stimulus categories is not unexpected.

Among the intrinsic components, the second and third (at low frequencies) are slightly lateralized and appear to represent the fronto-parietal attention networks. Unlike Brookes et al. (2011b), we did not find components describing the entire default mode network. We also could not find the cerebellar network that Brookes et al. (2011b) identified because we defined our source points on the cortical surface alone.

The putative orbitofrontal components seem to be related to eye-movement artifacts. This finding is not surprising considering that earlier studies have localized eye-blink artifacts to the orbit (Antervo et al., 1985). Although the correlations between EOG signal envelopes and the component envelope time courses are low, and the variance of the entire component cannot be explained by the EOG signals alone, caution must be exercised while interpreting these components as brain activity.

Methodological strengths and caveats

Advantages of eSFICA

As an alternative to envelope correlation, phase synchrony has been suggested as a mechanism for inter-areal communication (Fries, 2005). Future methods development efforts would have to strongly consider the importance of both envelope correlation and phase synchrony while studying inter-areal communication (see e.g., Hillebrand et al., 2012; Rosenberg-Katz et al., 2012). Whereas complex-valued methods such as TFICA or SFICA are equipped to reveal inter-areal phase synchrony, we did not find such components when these methods were applied to either simulated or real data (Hyvärinen et al., 2010; Ramkumar et al., 2012). One possible explanation is that phase synchrony is an intermittent phenomenon and is thus not robustly detectable with exploratory methods over time scales of minutes. Indeed, analysis in earlier studies reporting inter-areal phase-synchrony has typically been carried out trial by trial and over a time scale of hundreds of milliseconds to a few seconds (see e.g. Palva et al., 2009, 2010).

By contrast, eSFICA was able to find components with spatial maps showing bilateral networks such as the sensorimotor network, and a subset of the default mode network. Due to the real-valued nature of the method, the captured interactions are envelope correlations and they disregard phase interactions. In addition, since the ICs are zero-mean, it is possible to find envelope anti-correlations using this method. Finally, compared with the method applied by Brookes et al. (2011b), our method is automatically able to select relevant narrow frequency bands in a data-driven manner. As a result, the method can potentially find cross-frequency interactions within a single network.

Potential biases to the simulated data

Although we designed the simulated data set to closely mimic real MEG data, some artificial biases may still be present. For instance, increasing the temporal sparseness of the source time courses favors temporal ICA methods. To reduce this possible bias, we adjusted the temporal sparseness parameter so that the simulated time courses visually resembled real MEG data. In general, a number of measures exist to quantify the sparseness of a random variable, such as those based on the Lp-norm, $-\tanh$, and Gini coefficient (see e.g. Hurley and Rickard (2009)) and explicitly quantifying the sparseness of current estimates or invasive measurements would be useful for building more accurate simulations in future work.

Potential weaknesses in the group analysis

In this paper, we have adopted the standard approach of temporal concatenation across subjects (Beckmann and Smith, 2005; Calhoun et al., 2001). In general, temporal concatenation may create spurious correlations in the data. Although we are not aware of any work having shown such spurious correlations (whether linear or nonlinear) in the context of group ICA, such a possibility cannot be completely excluded. However, individual application of ICA on single-subject data, followed by post-hoc testing of consistency (Esposito et al., 2005; Hyvärinen, 2011; Langers, 2010; Hyvärinen and Ramkumar, 2013) would make fewer assumptions on the similarity of statistical properties of the data from different subjects. Optimizing the group analysis is certainly an avenue for future methodological development.

Other considerations

A number of weaknesses regarding the applicability of the algorithm and the uncertainty about the functional significance of estimated ICs remain to be addressed. First, although the STFT is a standard technique for spectral estimation, the estimates could potentially be improved with wavelet transforms. Selecting the scale of the wavelets or the window sizes for Fourier transforms could be empirically assessed based on

their influence on functional connectivity. Second, the choice of the number of independent components has been ascertained based on a rough heuristic. Although theoretical metrics exist to quantify the number of degrees of freedom in a dataset, as we have discussed elsewhere (Ramkumar et al., 2012) assessing the dimensionality of the dataset is confounded by the preprocessing step (SSS), as well as by source localization with MNE, followed by PCA. Careful empirical work similar to certain fMRI studies (Abou-Elseoud et al., 2010; Smith et al., 2009) using highly realistic simulations or a real MEG dataset would go a long way towards addressing this problem. Third, we have dealt with the problem of robust ICA estimation and inter-subject consistency by the standard approach of temporal concatenation across subjects (Beckmann and Smith, 2005; Calhoun et al., 2001). However, individual application of ICA on single-subject data, followed by post-hoc testing of consistency (Esposito et al., 2005; Hyvärinen, 2011; Langers, 2010) would make fewer assumptions on the similarity of statistical properties of the data from different subjects. Optimizing the group analysis is certainly an avenue for future methodological development.

Conclusion

We developed a data-driven method to characterize resting-state oscillatory brain networks at the cortical level across subjects. The identified RSNs were in agreement with those previously reported in the fMRI and MEG literature. Further, we showed that a majority of these RSNs were consistently modulated by external stimulation, while the 'intrinsic' networks remained seemingly unaffected by stimulation.

Acknowledgments

This study was supported by the Finnish Graduate School of Neuroscience, ERC (Advanced Grant #232946 to R. Hari), the Academy of Finland (Finnish Centre of Excellence Program 2006–2011) and the aivoAALTO project of Aalto University. We thank Riitta Hari for valuable comments on the manuscript.

References

Abou-Elseoud, A., Starck, T., Remes, J., Nikkinen, J., Tervonen, O., Kiviniemi, V., 2010. The effect of model order selection in group PICA. Hum. Brain Mapp. 31, 1207–1216.
Antervo, A., Hari, R., Katila, T., Ryhänen, T., Seppänen, M., 1985. Magnetic fields produced by eye-blinking. Electroencephalogr. Clin. Neurophysiol. 61, 247–253.
Beckmann, C.F., Smith, S.M., 2005. Tensorial extensions of independent component analysis for multisubject FMRI analysis. Neuroimage 25, 294–311.
Bingham, E., Hyvärinen, A., 2000. A fast fixed-point algorithm for independent component analysis of complex valued signals. Int. J. Neural Syst. 1–8.
Biswal, B., Yetkin, F.Z., Haughton, V.M., Hyde, J.S., 1995. Functional connectivity in the motor cortex of resting human brain using echo-planar MRI. Magn. Reson. Med. 34, 537–541.
Boonstra, T.W., Daffertshofer, A., Breakspear, M., Beek, P.J., 2007. Multivariate time–frequency analysis of electromagnetic brain activity during bimanual motor learning. Neuroimage 36, 370–377.
Brookes, M.J., Hale, J.R., Zumer, J.M., Stevenson, C.M., Francis, C.T., Barnes, G.R., Owen, J.P., Morris, P.G., Nagarajan, S.S., 2011a. Measuring functional connectivity using MEG: methodology and comparison with fcMRI. Neuroimage 56, 1082–1104.
Brookes, M.J., Woolrich, M., Price, D., Hale, J.R., Stephenson, M.C., Barnes, G.R., Smith, S.M., Morris, P.G., 2011b. Investigating the electrophysiological basis of resting-state networks using magnetoencephalography. Proc. Natl. Acad. Sci. U. S. A. 108, 16783–16788.
Buszaki, G., 2009. Rhythms of the Brain. Oxford University Press, USA.
Calhoun, V.D., Adali, T., Pearlson, G.D., Pekar, J.J., 2001. A method for making group inferences from functional MRI data using independent component analysis. Hum. Brain Mapp. 14, 140–151.
Chen, J.L., Ros, T., Gruzelier, J.H., 2013. Dynamic changes of ICA-derived EEG functional connectivity in the resting state. Hum. Brain Mapp. 34, 852–868.
Dalal, S.S., Guggisberg, A.G., Edwards, E., Sekihara, K., Findlay, A.M., Canolty, R.T., Berger, M.S., Kinght, R.T., Barbaro, N.M., Kirsch, H.E., Nagarajan, S.S., 2008. Neuroimage 40, 1686–1700.
Dale, A.M., Liu, A.K., Fischl, B.R., Buckner, R.L., Belliveau, J.W., Lewine, J.D., Halgren, E., 2000. Dynamic statistical parametric mapping: combining fMRI and MEG for high-resolution imaging of cortical activity. Neuron 26, 55–67.
Damoiseaux, J.S., Rombouts, S.A.R.B., Barkhof, F., Scheltens, P., Stam, C.J., Smith, S.M., Beckmann, C.F., 2006. Consistent resting-state networks across healthy subjects. Proc. Natl. Acad. Sci. U. S. A. 103, 13848–13853.
de Pasquale, F., Penna, S.D., Snyder, A.Z., Lewis, C., Mantini, D., Marzetti, L., Belardinelli, P., Ciancetta, L., Pizzella, V., Romani, G.L., Corbetta, M., 2010. Temporal dynamics of spontaneous MEG activity in brain networks. Proc. Natl. Acad. Sci. U. S. A. 107, 6040–6045.
Düzel, E., Habib, R., Schott, B., Schoenfeld, A., Lobaugh, N., McIntosh, A.R., Scholz, M., Heinze, H.J., 2003. A multivariate, spatiotemporal analysis of electromagnetic time–frequency data of recognition memory. Neuroimage 18, 185–197.
Esposito, F., Scarabino, T., Hyvärinen, A., Himberg, J., Formisano, E., Comani, S., Tedeschi, G., Goebel, R., Seifritz, E., Di Salle, F., 2005. Independent component analysis of fMRI group studies by self-organizing clustering. Neuroimage 25, 193–205.
Fischl, B., Sereno, M.I., Tootell, R.B., Dale, A.M., 1999. High-resolution intersubject averaging and a coordinate system for the cortical surface. Hum. Brain Mapp. 8, 272–284.
Fox, M.D., Raichle, M.E., 2005. Consistent resting-state networks across healthy subjects. Spontaneous fluctuations in the brain observed with functional magnetic resonance imaging. Nat. Rev. Neurosci. 8, 700–711.
Fries, P., 2005. A mechanism for cognitive dynamics: neuronal communication through neuronal coherence. Trends Cogn. Sci. 9, 474–480.
Giraud, A.L., Kleinschmidt, A., Poeppel, D., Lund, T.E., Frackowiak, R., Laufs, H., 2007. Endogeneous cortical rhythms determine hemispheric dominance for speech. Neuron 56, 1127–1134.
Goldman, R.I., Stern, J.M., Engel Jr., J., Cohen, M.S., 2002. Simultaneous EEG and fMRI of the alpha rhythm. Neuroreport 13, 2487–2492.
Hari, R., Salmelin, R., 1997. Human cortical oscillations: a view through the skull. Trends Neurosci. 20, 44–49.
Hillebrand, A., Barnes, G.R., Bosboom, J.L., Berendse, H.W., Stam, C.J., 2012. Frequency-dependent functional connectivity within resting-state networks: an atlas-based MEG beamformer solution. Neuroimage 59, 3909–3921.
Hoogenboom, N., Schoffelen, J.M., Oostenveld, R., Parkes, L.M., Fries, P., 2006. Localizing human visual gamma-band activity in frequency, time and space. Neuroimage 29, 764–773.
Hurley, N., Rickard, S., 2009. Comparing measures of sparsity. IEEE Trans. Inf. Theory 55, 4723–4742.
Hyvärinen, A., 2011. Testing the ICA mixing matrix based on inter-subject or inter-session consistency. Neuroimage 58, 132–136.
Hyvärinen, A., Ramkumar, P., 2013. Testing independent component patterns by inter-subject or inter-session consistency. Front. Hum. Neurosci. 7, 94.
Hyvärinen, A., Ramkumar, P., Parkkonen, L., Hari, R., 2010. Independent component analysis of short-time Fourier transforms for spontaneous EEG/MEG analysis. Neuroimage 49, 257–271.
Jensen, O., Tesche, C.D., 2002. Frontal theta activity in humans increases with memory load in a working memory task. Eur. J. Neurosci. 15, 1395–1399.
Knyazev, G.G., Slobodskoj-Plusnin, J.Y., Bocharov, A.V., Pylkova, L.V., 2011. The default mode network and EEG alpha oscillations: an independent component analysis. Brain Res. 1402, 67–69.
Langers, D.R.M., 2010. Unbiased group-level statistical assessment of independent component maps by means of automated retrospective matching. Hum. Brain Mapp. 31, 727–742.
Laufs, H., Krakow, K., Sterzer, P., Eger, E., Beyerle, A., Salek-Haddadi, A., Kleinschmidt, A., 2003. Electroencephalographic signatures of attentional and cognitive default modes in spontaneous brain activity at rest. Proc. Natl. Acad. Sci. U. S. A. 100, 11053–11058.
Malinen, S., Hlushchuk, Y., Hari, R., 2007. Towards natural stimulation in fMRI—issues of data analysis. Neuroimage 35, 131–139.
Mantini, D., Perrucci, M.G., Del Gratta, C., Romani, G.L., Corbetta, M., 2007. Electrophysiological signatures of resting state networks in the human brain. Proc. Natl. Acad. Sci. U. S. A. 104, 13170–13175.
Moosmann, M., Ritter, P., Krastel, I., Brink, A., Thees, S., Blankenburg, F., Taskin, B., Obrig, H., Villringer, A., 2003. Correlates of the alpha rhythm in functional magnetic resonance imaging and near infrared spectroscopy. Neuroimage 20, 145–158.
Nir, Y., Mukamel, R., Dinstein, I., Privman, E., Harel, M., Fisch, L., Gelbard-Sagiv, H., Kipervasser, S., Andelman, F., Neufeld, M.Y., Kramer, U., Arieli, A., Fried, I., Malach, R., 2008. Interhemispheric correlations of slow spontaneous neuronal fluctuations revealed in human sensory cortex. Nat. Neurosci. 11, 1100–1108.
Palva, S., Monto, S., Palva, J.M., 2009. Graph properties of synchronized cortical networks during visual working memory maintenance. Neuroimage 49, 3257–3268.
Palva, J.M., Monto, S., Kulashekhar, S., Palva, S., 2010. Neuronal synchrony reveals working memory networks and predicts individual memory capacity. Proc. Natl. Acad. Sci. U. S. A. 107, 7580–7585.
Ramkumar, P., Parkkonen, L., Hari, R., Hyvärinen, A., 2012. Characterization of neuromagnetic brain rhythms over time scales of minutes using spatial independent component analysis. Hum. Brain Mapp. 33, 1648–1662.
Rosenberg-Katz, K., Jamshy, S., Singer, N., Podlipsky, I., Kipervasser, S., Andelman, F., Neufeld, M.Y., Intrator, N., Fried, I., Hendler, T., 2012. Enhanced functional synchronization of medial and lateral PFC underlies internally-guided action planning. Front. Hum. Neurosci. 6.
Smith, S.M., Fox, P.T., Miller, K.L., Glahn, D.C., Fox, P.M., Mackay, C.E., Filippini, N., Watkins, K.E., Toro, R., Laird, A.R., Beckmann, C.F., 2009. Correspondence of the brain's functional architecture during activation and rest. Proc. Natl. Acad. Sci. U. S. A. 106, 13040–13045.
Stone, J.V., Porrill, J., Porter, N.R., Wilkinson, I.D., 2002. Spatiotemporal independent component analysis of event-related fMRI data using skewed probability density functions. Neuroimage 15, 407–421.
Taulu, S., Kajola, M., 2005. Presentation of electromagnetic multichannel data: the signal space separation method. J. Appl. Phys. 97, 124905–124910.
Tiihonen, J., Hari, R., Kajola, M., Karhu, J., Ahlfors, S., Tissari, S., 1991. Magnetoencephalographic 10-Hz rhythm from the human auditory cortex. Neurosci. Lett. 129, 303–305.